DIFFUSEVAE: EFFICIENT, CONTROLLABLE AND HIGH-FIDELITY GENERATION FROM LOW-DIMENSIONAL LATENTS

Kushagra Pandey
Indian Institute of Technology, Kanpur
kushagrap20@iitk.ac.in

Avideep Mukherjee
Indian Institute of Technology, Kanpur
avideep@cse.iitk.ac.in

Piyush Rai
IIT Kanpur and Google Research
piyush@cse.iitk.ac.in

Abhishek Kumar
Google Research
abhishk@google.com

ABSTRACT

Diffusion Probabilistic models have been shown to generate state-of-the-art results on several competitive image synthesis benchmarks but lack a low-dimensional, interpretable latent space, and are slow at generation. On the other hand, Variational Autoencoders (VAEs) typically have access to a low-dimensional latent space but exhibit poor sample quality. Despite recent advances, VAEs usually require high-dimensional hierarchies of the latent codes to generate high-quality samples. We present DiffuseVAE, a novel generative framework that integrates VAE within a diffusion model framework, and leverage this to design a novel conditional parameterization for diffusion models. We show that the resulting model can improve upon the unconditional diffusion model in terms of sampling efficiency while also equipping diffusion models with the low-dimensional VAE inferred latent code. Furthermore, we show that the proposed model can generate high-resolution samples and exhibits synthesis quality comparable to state-of-the-art models on standard benchmarks. Lastly, we show that the proposed method can be used for controllable image synthesis and also exhibits out-of-the-box capabilities for downstream tasks like image super-resolution and denoising. For reproducibility, our source code is publicly available at https://github.com/kpandey008/DiffuseVAE.[1]

1 Introduction

Generative modeling is the task of capturing the underlying data distribution and learning to generate novel samples from a posited explicit/implicit distribution of the data in an unsupervised manner. Variational Autoencoders (VAEs) [27, 45] are a type of explicit-likelihood based generative models which are often also used to learn a low-dimensional latent representation for the data. The resulting framework is very flexible and can be used for downstream applications, such as learning disentangled representations [5, 9, 20], semi-supervised learning [28], anomaly detection [43], among others. However, in image synthesis applications, VAE generated samples (or reconstructions) are usually blurry and fail to incorporate high-frequency information [14]. Despite recent advances [10, 44, 56, 60, 62] in improving VAE sample quality, there is still a significant gap in sample quality between VAEs and their implicit-likelihood counterparts like GANs [17, 23, 24, 25] with all these advanced models requiring a much larger dimensional latent space.

In contrast, denoising diffusion probabilistic models (DDPM) [21, 50] have been shown to achieve impressive performance on several image synthesis benchmarks, even surpassing GANs on several such benchmarks [13, 22]. However, conventional diffusion models require an expensive iterative sampling procedure and lack a low-dimensional latent representation, limiting these models' practical applicability for downstream applications.

[1] Preprint. Work in Progress

Figure 1: DiffuseVAE can generate high-fidelity samples from low-dimensional latents with lesser number of timesteps in the reverse process. (Left) Selected 128 x 128 samples (Top) generated from a continuous noise conditioned DiffuseVAE model trained on the CelebAMask-HQ dataset. The corresponding Stage-1 VAE samples are shown in the Bottom row. DiffuseVAE samples were generated using 10 timesteps in the reverse process and a VAE latent code dimension of 1024. (Right) Selected unconditional CIFAR-10 samples generated from a continuous noise conditioned DiffuseVAE model using 50 timesteps (Top) and 100 timesteps (Bottom) with a VAE latent code size of 512. The generation is entirely driven by low dimensional latents – the diffusion process latents are fixed and shared between samples after the model is trained (See Section 5.2 for more details).

In this work, we present DiffuseVAE, a novel framework which combines the best of both VAEs and DDPMs in an attempt to alleviate the aforementioned issues with both types of model families. We present a novel two-stage conditioning framework where in the first stage, any arbitrary conditioning signal y can be first modeled using a single stochastic layer VAE. In the second stage, we can then model the training data x using a DDPM conditioned on y and the low-dimensional VAE latent code representation of y. We show that, coupled with some simplifying assumptions, our framework reduces to a simple scheme of fitting a VAE on the training data (x) in the first stage followed by modeling x in the second stage using a DDPM conditioned on the VAE reconstructions ($\hat{x}$) of the training data. The main contributions of our work can be summarized as follows:

1. **A novel conditioning framework**: We propose a generic DiffuseVAE conditioning framework and show that our framework can be reduced to a simple *generator-refiner* framework in which blurry samples generated from a VAE are *refined* using a conditional DDPM formulation (See Fig.1). This effectively equips the diffusion process with a low dimensional latent space and we observe that noise latents in the diffusion process have very little information for the generation. We explore two types of conditioning formulations in the second stage DDPM model and show that both perform comparably with no significant advantages of one over the other.
2. **Controllable synthesis from a low-dimensional latent**: We show that DiffuseVAE is able to generate high-quality samples with performance comparable to recent generative models on standard benchmarks like CIFAR-10. More importantly, DiffuseVAE generated samples can be controlled directly using the low-dimensional VAE latent space, and noise of the diffusion process has very little impact on the generation. To the best of our knowledge, this is the first work to show high fidelity generation using a low dimensional latent space with a model trained using a non-adversarial objective.
3. **Sampling speedups**: We show that DiffuseVAE inherently requires fewer reverse diffusion sampling steps during inference compared to the unconditional DDPM model. Furthermore we also present a DiffuseVAE formulation conditioned on continuous noise as proposed in [8] and show that we can generate plausible samples in as few as **10** reverse sampling steps.
4. **Generalization to auxiliary tasks**: We show that DiffuseVAE exhibits out-of-the-box generalization to downstream tasks like image super-resolution and denoising.
5. **State of the art comparisons**: We show that DiffuseVAE outperforms existing VAE-based generative models and many GAN-based models on standard image-synthesis benchmarks.

2 Background

2.1 Variational Autoencoders

VAEs [27, 45] are based on a simple but principled encoder-decoder based formulation which tries to maximize the evidence lower bound (ELBO) of the data log-likelihood, which is intractable to compute in general. The VAE

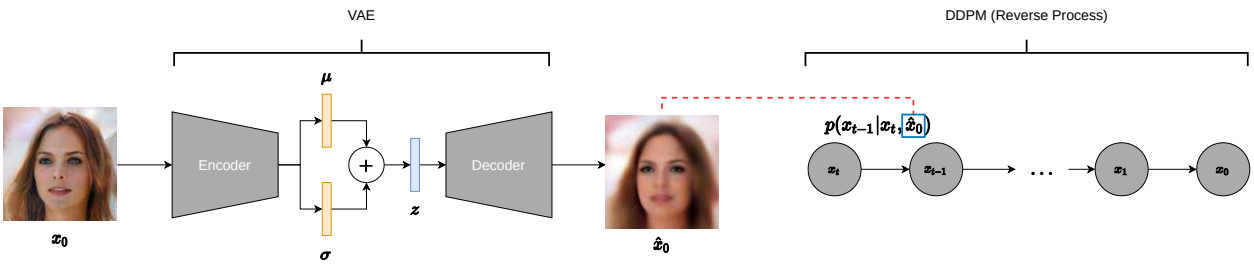

Figure 2: Proposed DiffuseVAE generative process under the simplifying design choices discussed in Section 3.2. In this setting, the VAE encoder takes the original image x_0 as input. The DDPM reverse process in the second stage is conditioned on the VAE reconstruction obtained in the first stage as discussed in Section 3.2.

optimization objective can be stated as follows:

$$\mathcal{L}(\theta, \phi) = \mathbb{E}_{q_\phi(z|x)}[\log p_\theta(x|z)] - \mathcal{D}_{KL}[q_\phi(z|x)\|p(z)] \tag{1}$$

Under the amortized variational inference scheme, the approximate posterior ($q_\phi(z|x)$) and the likelihood ($p_\theta(x|z)$) distributions can be modeled using deep neural networks with parameters ϕ and θ, respectively using the reparameterization trick [27, 45]. The choice of the prior distribution $p(z)$ is flexible and can vary from a standard Gaussian [27] to more expressive priors like normalizing flows [18, 29, 58].

2.2 Denoising Diffusion Probabilistic Models

DDPMs [21, 50] are latent-variable models consisting of a forward noising process ($q(x_{1:T}|x_0)$) which gradually destroys the structure of the data x_0 and a reverse denoising process (($p(x_{0:T})$)) which learns to recover the original data x_0 from the noisy input. The forward noising process is modeled using a first-order Markov chain with Gaussian transitions and is fixed throughout training, and the noise schedules β_1 to β_T can be fixed or learned. The form of the forward process can be summarized as follows:

$$q(x_{1:T}|x_0) = \prod_{t=1}^{T} q(x_t|x_{t-1}) \tag{2}$$

$$q(x_t|x_{t-1}) = \mathcal{N}(\sqrt{1-\beta_t}x_{t-1}, \beta_t I) \tag{3}$$

The reverse process can also be parameterized using a first-order Markov chain with a learned Gaussian transition distribution as follows

$$p(x_{0:T}) = p(x_T) \prod_{t=1}^{T} p_\theta(x_{t-1}|x_t) \tag{4}$$

$$p_\theta(x_{t-1}|x_t) = \mathcal{N}(\mu_\theta(x_t, t), \Sigma_\theta(x_t, t)) \tag{5}$$

Given a large enough T and a well-behaved variance schedule of β_t, the distribution $q(x_T|x_0)$ will approximate an isotropic Gaussian. We can generate a new sample from the underlying data distribution $q(x_0)$ by sampling a latent from $p(x_T)$ (chosen to be an isotropic Gaussian distribution) and running the reverse process. We highly encourage the readers to refer to Appendix A for a more detailed background on diffusion models.

3 DiffuseVAE: VAEs meet Diffusion Models

3.1 DiffuseVAE Training Objective

Given a high-resolution image x_0, an auxiliary conditioning signal y to be modelled using a VAE, a latent representation z associated with y, and a sequence of T representations $x_{1:T}$ learned by a diffusion model, the DiffuseVAE joint distribution can be factorized as:

$$p(x_{0:T}, y, z) = p(z)p_\theta(y|z)p_\phi(x_{0:T}|y, z) \tag{6}$$

where θ and ϕ are the parameters of the VAE decoder and the reverse process of the conditional diffusion model, respectively. Furthermore, since the joint posterior $p(x_{1:T}, z|y, x_0)$ is intractable to compute, we approximate it using a surrogate posterior $q(x_{1:T}, z|y, x_0)$ which can also be factorized into the following conditional distributions:

$$q(x_{1:T}, z|y, x_0) = q_\psi(z|y, x_0)q(x_{1:T}|y, z, x_0) \tag{7}$$

where ψ are the parameters of the VAE recognition network ($q_\psi(z|y, x_0)$). As considered in previous works [21, 50] we keep the DDPM forward process ($q(x_{1:T}|y, z, x_0)$) fixed throughout training. The log-likelihood of the training data can then be obtained as:

$$\log p(x_0, y) = \log \int p(x_{0:T}, y, z) dx_{1:T} dz \tag{8}$$

Since this estimate is intractable to estimate analytically, we optimize the ELBO corresponding to the log-likelihood. It can be shown that the log-likelihood estimate of the data can be approximated using the following lower bound (See Appendix B.1 for the proof)

$$\begin{aligned} \log p(x_0, y) \geq & \underbrace{\mathbb{E}_{q_\psi(z|y,x_0)}[p_\theta(y|z)] - \mathcal{D}_{KL}(q_\psi(z|y, x_0)||p(z))}_{\mathcal{L}_{\text{VAE}}} + \\ & \mathbb{E}_{z\sim q(z|y,x_0)}\left[\underbrace{\mathbb{E}_{q(x_{1:T}|y,z,x_0)}\left[\frac{p_\phi(x_{0:T}|y, z)}{q(x_{1:T}|y, z, x_0)}\right]}_{\mathcal{L}_{\text{DDPM}}}\right] \end{aligned} \tag{9}$$

We next discuss the choice of the conditioning signal y, some simplifying design choices and several parameterization choices for the VAE and the DDPM models.

3.2 Simplifying design choices

In this work we are interested in unconditional modeling of data. To this end, we make the following simplifying design choices:

1. We assume the conditioning signal y to be x_0 itself which ensures a deterministic mapping between y and x_0. Given this choice, we do not condition the reverse diffusion process on y and take it as $p_\phi(x_{0:T}|z)$.
2. For ease of optimization, we train Eq. (9) in a sequential two-stage manner i.e. first optimizing $\mathcal{L}_{\text{VAE}}$ and then optimize for $\mathcal{L}_{\text{DDPM}}$ while fixing θ and ψ.
3. Lastly, instead of conditioning the reverse diffusion directly on the latent code z, we condition the second stage DDPM model on the VAE reconstruction $\hat{x}_0$ which is a deterministic function of z. The choice of conditioning on $\hat{x}_0$ (same size as the original image) instead of z (usually lower-dimensional) allows us to condition the second stage DDPM directly on samples drawn from another model (not necessarily VAE) or on real images, which can be quite useful as illustrated in Section 5.4.

With these design choices, as shown in Fig. 2, the DiffuseVAE training objective reduces to simply training a VAE model on the training data x_0 in the first stage and conditioning the DDPM model on the VAE reconstructions in the second stage. We next discuss the specific parameterization choices for the VAE and DDPM models.

3.3 VAE parameterization

In this work we only consider the standard VAE (with a single stochastic layer) as discussed in Section 2.1. However, due to the flexibility of the DiffuseVAE two-stage training, more sophisticated, multi-stage VAE approaches as proposed in [10, 44, 56] can also be utilized to model the input data x_0.

3.4 DDPM parameterization

In this section, we discuss the two types of DDPM formulations considered in this work.

3.4.1 Formulation 1

In this formulation, we make the following simplifying assumptions:

1. We assume that the forward process is independent of the VAE reconstructions $\hat{x}$ and the latent code information z i.e. $q(x_{1:T}|z, x_0) \approx q(x_{1:T}|x_0)$.

2. The reverse process transitions are conditionally dependent on only the VAE reconstruction, i.e., $p(x_{0:T}|z) \approx p(x_{0:T}|\hat{x}_0)$

A similar parameterization has been considered in recent work on conditional DDPM models [22, 47]. We concatenate the VAE reconstruction to the reverse process representation x_t at each time step t to obtain x_{t-1}.

3.4.2 Formulation 2

In this formulation, we make the following simplifying assumptions:

1. The forward process transitions are conditionally dependent on the VAE reconstruction, i.e., $q(x_{1:T}|z, x_0) \approx q(x_{1:T}|\hat{x}_0, x_0)$
2. The reverse process transitions are conditionally dependent on only the VAE reconstruction, i.e., $p(x_{0:T}|z) \approx p(x_{0:T}|\hat{x}_0)$

More specifically, we design the forward process transitions to incorporate the VAE reconstruction $\hat{x}_0$ as follows:

$$q(x_1|x_0, \hat{x}_0) = \mathcal{N}(\sqrt{1-\beta_1}x_0 + \hat{x}_0, \beta_1 I) \tag{10}$$

$$q(x_t|x_{t-1}, \hat{x}_0) = \mathcal{N}(\sqrt{1-\beta_t}x_{t-1} + (1-\sqrt{1-\beta_t})\hat{x}_0, \beta_t I) \qquad \text{where} \quad t > 1$$

It can be shown that the forward conditional marginal in this case becomes (See Appendix B.2 for proof):

$$q(x_t|x_0, \hat{x}_0) = \mathcal{N}(\sqrt{\bar{\alpha}_t}x_0 + \hat{x}_0, (1-\bar{\alpha}_t)I) \tag{11}$$

For $t = T$ and a *well-behaved* noise schedule β_t, $\bar{\alpha}_T \approx 0$ which implies $q(x_T|x_0, \hat{x}_0) \approx \mathcal{N}(\hat{x}_0, I)$. Intuitively, this means that the Gaussian $\mathcal{N}(\hat{x}_0, I)$ becomes our base measure ($p(x_T)$) during inference on which we need to run our reverse process. Since the simplified denoising training formulation proposed in [21] depends on the functional form of the forward process posterior $q(x_{t-1}|x_t, x_0)$, this formulation results in several modifications in the standard DDPM training and inference which are discussed in detail in Appendix C.

It is worth noting that, in principle, it is also possible to condition the forward and the reverse processes for both the DDPM formulations with the VAE latent code information z in addition to the reconstruction $\hat{x}_0$. However we do not consider such a conditioning scheme in this work.

4 Related Work

Following the seminal work of [21, 50] on diffusion models, there has been a lot of recent progress in both unconditional [13, 30, 38] and conditional diffusion models [8, 11, 22, 47] (including score-based models [52, 54], based on a connection proposed in [21]) for a variety of downstream tasks including image synthesis, audio synthesis and likelihood estimation among others. Recent work in DDPMs also includes speeding up the DDPM sampling process [35, 51, 61]. Similarly for VAEs [27, 45], there has also been progress in improving the ELBO estimates [4, 36, 49] and image synthesis [10, 33, 56, 62]. Next, we compare our proposed approach in detail with several of these related existing model families.

Unconditional DDPM: DDPM as introduced in [21] generates images unconditionally and lacks a low-dimensional latent code which makes limits the application scope of these models. On the other hand, we show that the proposed DiffuseVAE model can be used for tasks like image enhancement, super-resolution, etc. and the generated samples can be directly controlled using a low-dimensional latent space. Moreover, we show that under standard settings our approach requires fewer number of reverse process steps in general to produce plausible samples.

Conditional DDPM: Conditional DDPM as introduced in [22] and [47] uses multiple diffusion models for generating high-resolution images in a cascaded fashion. However, for even a two-stage pipeline, the sampling time of such models would be effectively much higher than DiffuseVAE. Given the flexibility of our approach, we hypothesize that a single-stage VAE can also be replaced by a complex multi-stage VAE architecture as proposed in [10, 56] for comparable sample quality to cascaded diffusion models without affecting the sampling time significantly. Moreover, such cascades lack a low-dimensional latent code which might be a limiting factor for certain downstream applications. It is worth noting that, [22] use a conditioning augmentation scheme where the high-resolution image is generated by conditioning on a blurred/noisy low resolution image. This augmentation scheme is empirically chosen and can be sub-optimal across datasets. In contrast, our model is conditioned on a reconstruction generated by a VAE and no

(a) Formulation-1 (b) Formulation-2

Figure 3: Illustration of the generator-refiner framework in DiffuseVAE. The VAE generated samples (Bottom row) are refined by the Stage-2 DDPM model.

explicit augmentation is required.

VAE based methods Hierarchical VAEs [10, 44, 55, 56] can suffer from posterior collapse and heuristics like gradient skipping and spectral normalization [37] might be required to stabilize training. Moreover, these models require a large dimensionality of the latent codes to generate high-fidelity samples [44, 56]. In contrast, DiffuseVAE training does not suffer from such instabilities and the proposed method requires a single latent code layer (with dimensionality comparable to GANs) to generate high-fidelity samples. Among other recent works, VAEBM [62] uses EBMs [15, 39] to refine VAE samples while LSGM [56] perform score-based modeling in the latent space of a VAE backbone. However, both VAEBM and LSGM used NVAE [56] as the base VAE architecture which also lacks a low-dimensional latent code. [33] *distill* the disentanglement properties in the VAE latent code to the latent space of a GAN-based generator. However, this approach would also suffer from existing problems of training stability and mode-collapse in GAN-based models. On the other hand, DiffuseVAE does not suffer from such problems.

5 Experiments

We evaluate the effectiveness of our method by making qualitative and quantitative comparisons between the proposed DiffuseVAE framework and the unconditional DDPM model [21] on CIFAR10 [31] and the CelebAMask-HQ [32] datasets. Unless specified otherwise, we used CelebAMask-HQ images at the 128 x 128 resolution. For all the experiments, we set the number of diffusion timesteps (T) to 1000 during training. The noise schedule in the DDPM forward process was set to a linear schedule between $\beta_1 = 10^{-4}$ and $\beta_2 = 0.02$ during training. We use our unconditional DDPM implementation as a comparison baseline. We computed the FID [19] score using 5k samples for all experiments except for state-of-the-art comparisons for which we used 50k samples. More details regarding the network architecture and the training hyperparameters can be found in Appendix D.

5.1 Generator-refiner framework

Fig. 3 shows samples generated from the proposed DiffuseVAE model trained on the CelebAMask-HQ dataset and their corresponding Stage-1 VAE reconstructions. For both DiffuseVAE formulations-1 and 2, DiffuseVAE generated samples (Fig. 3 (Top row) are a refinement of the *blurry* samples generated by our single-stage VAE model (Bottom row). This observation qualitatively validates our *generator-refiner* framework in which the Stage-1 VAE model acts as a generator and the Stage-2 DDPM model acts as a refiner. Additional samples illustrating the same can be found in Appendix E.

5.2 Controllable synthesis via low-dimensional DiffuseVAE latents

DiffuseVAE Interpolation: The proposed DiffuseVAE model consists of two types of latent representations: the low-dimensional VAE latent code z_{vae} and the DDPM intermediate representations $x_{1:T}$ associated with the DDPM reverse process (which are of the same size of the input image x_0 and thus might not be beneficial for downstream tasks). We next discuss the effects of manipulating both z_{vae} and x_T. We consider the following two interpolation settings:

(a) DiffuseVAE samples generated from formulations-1 and 2 by interpolating in the VAE latent space.

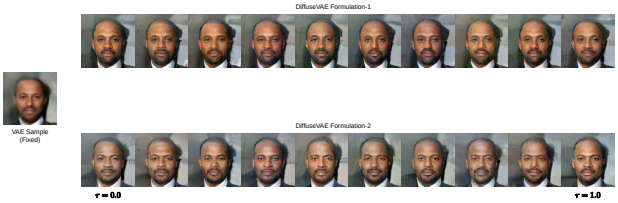

(b) DiffuseVAE samples generated from formulations-1 and 2 by interpolating in the DDPM latent space with a fixed VAE reconstruction.

Figure 4: Interpolation in DiffuseVAE. τ denotes the linear interpolation factor. (Best viewed with zoom-in)

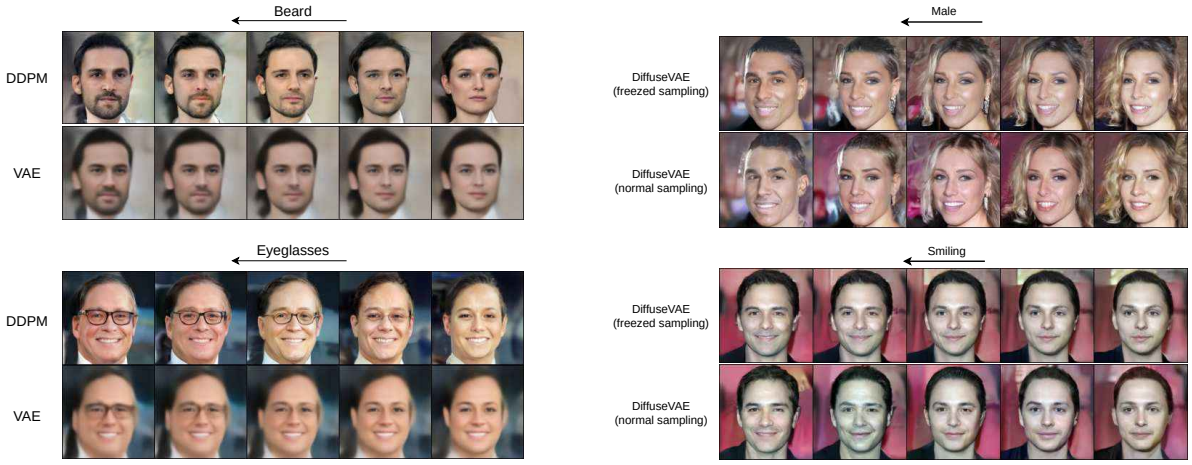

(a) (b)

Figure 5: (a) Interpolations in the VAE latent space along meaningful directions for controllable synthesis of DiffuseVAE (Formulation-1) generated samples. (b) Fixing the DDPM stochasticity improves controllable synthesis interpolations using DiffuseVAE. (Best viewed with zoom-in)

1. **Varying z_{vae} with fixed x_T**: We first sample two VAE latent codes $z_{vae}^{(1)}$ and $z_{vae}^{(2)}$ using the standard Gaussian distribution. We then perform linear interpolation between $z_{vae}^{(1)}$ and $z_{vae}^{(2)}$ to obtain intermediate VAE latent codes $\tilde{z}_{vae} = \tau z_{vae}^{(1)} + (1-\tau) z_{vae}^{(2)}$, which are then used to generate the corresponding DiffuseVAE samples with a shared intial x_T.
2. **Fixed z_{vae} with varying x_T**: Next, we sample the VAE latent code z_{vae} using the standard Gaussian distribution. With a fixed z_{vae}, we then sample two initial DDPM representations $x_T^{(1)}$ and $x_T^{(2)}$ from the reverse process base measure $p(x_T)$. We then perform linear interpolation between $x_T^{(1)}$ and $x_T^{(2)}$ with a fixed z_{vae} to generate the final DiffuseVAE samples.

Fig. 4a shows the DiffuseVAE generated samples with a fixed x_T and the interpolated z_{vae} while Fig 4b shows the DiffuseVAE generated samples with a fixed z_{vae} and the interpolated x_T. As can be observed, interpolating in the low-dimensional VAE latent space leads to changes in major features of the generated samples while changes in the DDPM latent conditioned on the same VAE reconstructions leads to minor changes in the DDPM reconstructions which can be attributed to the stochastic nature of the DDPM sampling procedure. This observation implies that the low-dimensional VAE latent code mostly controls the diversity of the generated samples and has more entropy than the DDPM representations x_T, which carry little semantic information. This implies that the low-dimensional VAE latent code inferred from the first stage can still be utilized in downstream tasks without compromising on sample quality. The resulting latent code can also be utilized to control DiffuseVAE sample synthesis which we next discuss.

Controllable Generation: We next perform interpolations in the low-dimensional VAE latent space along inferred directions representing specific concepts like gender, hair color etc. to generate controlled samples using DiffuseVAE. Fig. 5a visualizes DiffuseVAE interpolations across two such directions: *Male* and *Smiling*. Intuitively, these results

# of steps	DDPM (Unconditional)	DiffuseVAE (Form-1)	DiffuseVAE (Form-2)
200	418.33	263.96	270.59
300	293.34	88.95	86.44
400	143.20	33.15	34.43
500	74.69	25.37	25.37
1000	**14.23**	**22.78**	**22.95**

Table 1: FID (5k samples) score vs number of revserse sampling steps comparison between the Unconditional DDPM [21] and DiffuseVAE on the CelebAMask-HQ dataset

# steps	$\lambda = 1.0$	$\lambda = 0.5$	$\lambda = 0.1$
Formulation-1			
200	263.97	52.99	**42.59**
300	88.95	**30.33**	30.92
400	33.15	**26.49**	27.25
500	25.37	**24.70**	25.06
Formulation-2			
200	270.59	55.27	**46.79**
300	86.44	**31.72**	36.84
400	34.43	**27.12**	27.90
500	25.37	**25.14**	25.64

Table 2: Effect of temperature scaling on the DiffuseVAE sampling speed for the CelebAMask-HQ dataset (FID on 5k samples)

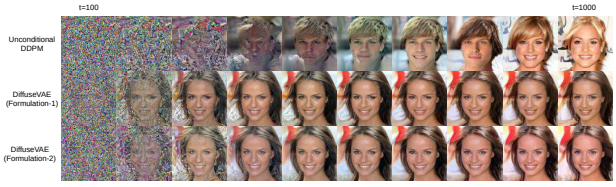

(a) Comparison between samples generated from the unconditional DDPM and DiffuseVAE (formulations 1 and 2) vs the number of sampling steps.

(b) Effect of temperature (λ) on DiffuseVAE reverse process sampling for DiffuseVAE (formulation-1)

Figure 6: Qualitative analysis of the sampling speed-ups in DiffuseVAE. The time t denotes the number of reverse process steps performed during inference. The samples were obtained at equidistant time points between t=100 and t=1000. (Best viewed with zoom-in)

can be expected since the DDPM model in the second stage only refines the VAE generated samples while the semantic meaning is still preserved in the VAE inferred latent space.

It is worth noting that the directions for these concepts were obtained by empirically averaging the latent codes of a subset of ground-truth images in the CelebAMask-HQ dataset containing these attributes. An attribute positive image was then obtained by adding the averaged attribute latent vector to the latent code of a attribute negative VAE sample followed by decoding the resulting latent vector. The interpolations were then obtained by linearly interpolating between the positive and the negative latent codes. Some additional interpolation results are provided in Appendix E.

Handling the DDPM stochasticity: Even though the diversity of the generated image samples from DiffuseVAE is primarily controlled from the low-dimensional VAE latent code, the stochasticity in the second stage DDPM sampling process can occasionally result in artifacts which might be undesirable in downstream applications like image manipulation etc. This is evident in some of our results (See Fig. 4a, 5a) where sudden changes in minor attributes (like skin-color, hair-color etc.) can be clearly observed. To make the samples generated from DiffuseVAE deterministic (i.e. controllable only from z_{vae}), we randomly sample and store the initial DDPM latent (x_T) and z_t generated at each sampling step in DDPM reverse process sampling. We then use these stored representations in the Stage-2 DDPM sampling for all generated samples. We noticed that this simple technique added more consistency in our latent interpolations (See Fig. 5b to observe the differences between controllable interpolations with (Top Row) and without (Bottom row) using this technique for two attributes *Male* and *Smiling*). The quantitative effects of this design choice are discussed in details in Section 5.3.

5.3 Sampling speedups with DiffuseVAE

DiffuseVAE inherently requires fewer sampling steps than the unconditional DDPM: Under standard training and inference settings, we qualitatively compare the unconditional DDPM model proposed in [21] and DiffuseVAE in

# steps	Noise schedule	DiffuseVAE (Form-1)	DiffuseVAE (Form-2)
10	Linear(1e-6, 0.8)	34.97	**33.71**
10	Linear(1e-6, 0.7)	34.51	**33.41**
25	Linear(1e-6, 0.6)	30.88	**29.61**
50	Linear(1e-6, 0.3)	29.35	**28.45**

Table 3: FID score (5k samples) comparison between DiffuseVAE formulations 1 and 2 when using continuous noise conditioning for different inference schedules. No temperature scaling was used.

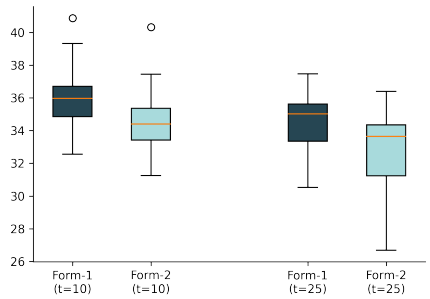

Figure 7: FID score comparison (5k samples) between DiffuseVAE formulations-1 and 2 conditioned on continuous noise for t=10 and 25 inference steps with shared DDPM latents.

terms of the number of reverse process sampling steps required to produce high-fidelity samples. Fig. 6a shows the samples generated from the unconditional DDPM (Top) and the samples generated using DiffuseVAE formulations 1 (Middle) and 2 (Bottom). The visualization in Fig. 6a and the quantitative results in Table 1 suggests that DiffuseVAE requires around **half** the number of steps to generate plausible samples than an unconditional DDPM model which starts generating plausible samples around $t = 1000$. It is worth noting that this property is intrinsic to DiffuseVAE as the model was not specifically designed to reduce the number of reverse process sampling steps during inference.

However, it is worth noting that the unconditional DDPM model outperforms DiffuseVAE at $t = 1000$ (See Table 1). We hypothesize that this gap in performance can be reduced by training the VAE prior as done in previous works [44, 59] since VAEs can generate out-of-distribution samples during inference due to the mismatch between the aggregated posterior $q(z)$ and the prior $p(z)$ [2, 12, 16] which after DDPM refinement can affect the FID scores negatively.

Effect of temperature scaling: During inference, it is common to scale the standard deviation of the base Gaussian distribution by λ to obtain better quality samples at the expense of image diversity [26, 56]. However, a similar scaling technique has not been explored much in diffusion models. Moreover, [57] state that temperature scaling hurts the generation quality when performing score-based modelling in the VAE latent space.

In this work, we experiment with a temperature scaling technique where during the DDPM sampling stage in DiffuseVAE, we sample the initial DDPM latent x_T from a base Gaussian distribution with standard deviation scaled by λ for both formulations 1 and 2. The resulting DiffuseVAE reverse process generations with formulation-1 for different λ values are visualized in Fig 6b with quantitative FID scores summarized in Table 2. We observe that for decreasing values of λ we get better DDPM refinements during the early reverse process sampling phase with a large increase improvement in FID scores at $t = 200$ and $t = 300$ steps. More interestingly, when using temperature scaling, the FID scores at around $t = 300$ steps are better than $t = 400$ steps. Similarly the FID scores at $t = 400$ steps is comparable to FID scores at $t = 500$. Thus, DiffuseVAE provides a way to reduce the number of sampling steps further using temperature scaling without hurting the sample diversity which is primarily controlled from the VAE latent space. It is worth noting that this type of scaling cannot be applied to the conventional DDPM. However, lowering λ to 0.1 (or below) leads to diminishing returns except at $t = 200$ steps.

Continuous noise conditioning in DiffuseVAE: Recently [8] proposed an alternative way to train DDPMs for speech synthesis where the reverse process neural network is conditioned on the continuous noise scales sampled from a piecewise uniform distribution. This allows the network to generalize to unseen noise schedules during training, further allowing to design noise schedules over a fewer number of steps during sampling. However, the extension of this form of conditioning for images remains under-explored in diffusion models. [47] explored continuous noise conditioning for images in the context of image super-resolution but do not provide much analysis in terms of quantitative measures.

To assess the computational benefits of this form of conditioning during inference for image data, we train DiffuseVAE (both formulations 1 and 2) with continuous noise conditioning. A comparison of FID scores for different noise schedules designed during inference are shown in Table 3. For this form of conditioning we find that formulation-2 performs slightly better than formulation-1. Despite a notable difference between the FID scores for different inference

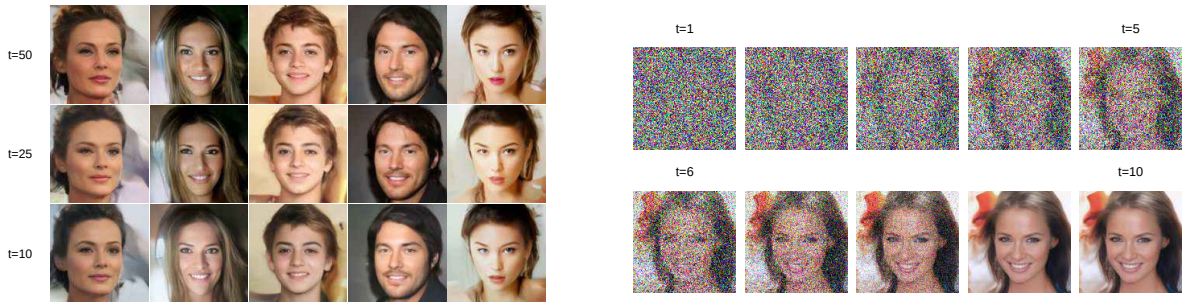

(a) (b)

Figure 8: (a) Visualization of DiffuseVAE (Form-1) samples when conditioned on cont. noise at t=50, 25 and 10 steps. (b) Samples visualized at each step during sampling from a 10-step DiffuseVAE (Form-1) model conditioned on continuous noise. (Best viewed with zoom-in)

Figure 9: DiffuseVAE (Formulation-1) generalization to auxiliary tasks like Image super-resolution (Left) and Image denoising (Right)

schedules, we found minimal perceptual differences between the generated samples for $t = 50$ and $t = 10$ or $t = 25$ suggesting the computational benefit of this form of conditioning. Some qualitative samples generated using DiffuseVAE (formulation-1) conditioned on the noise for 10 steps are shown in Fig. 8a (Bottom Row) and the individual reverse sampling steps for a sample are shown in Fig. 8b (See Appendix E for additional samples).

We also report a quantitative analysis of the effect of fixing DDPM latents across generated samples by comparing the FID scores (on 5k samples) between DiffuseVAE formulations-1 and 2 conditioned on continuous noise. For a given inference noise schedule and a DiffuseVAE formulation, we compute the FID score by generating DiffuseVAE samples with shared DDPM latents (sampled from a fixed random seed). Fig. 7 shows a boxplot comparison between FID scores across DiffuseVAE formulations and inference schedules for 10 such trials. The random seed for generating Stage-1 VAE samples is fixed across all trials. The results suggest that fixing DDPM latents across samples can improve or degrade the sample quality and can be unpredictable in this regard. Thus, design of stronger conditioning formulations to alleviate stochasticity in DDPM generated samples can be an interesting direction for future work.

5.4 Generalization to downstream tasks

Recently, [47] showed impressive image super-resolution results using diffusion models. However, such a model is trained explicitly for a single task and may not generalize to other forms of noise in the image. To test if our generator-refiner framework can generalize over different types of noisy inputs, we condition the second stage DDPM model (pre-trained on the CelebAMask-HQ dataset) on the noisy input (instead of the VAE reconstruction). Moreover, for this experiment we utilize generated samples from StyleGAN2 [25] trained on the FFHQ dataset [24].

The samples obtained from such conditioning are visualized in Fig. 9. On a 64 x 64 to 128 x 128 image super-resolution task, our model is able to generate plausible refinements (Fig. 9 (Bottom row)) when compared to the original generated

	Method	FID ↓	IS ↑
Ours	DiffuseVAE (t=1000)	8.72	8.63 ± 0.06
	DiffuseVAE (t=500)	9.72	8.53 ± 0.11
	DiffuseVAE (t=100) (Cont. Noise)	11.71	8.27 ± 0.01
	DDPM (t=1000) [21]	3.90	9.34 ± 0.07
	DDPM (t=500) [21]	14.31	9.04 ± 0.11
VAE-based methods	VAEBM [62] (w/ PC)	12.19	8.43
	DC-VAE [42]	17.90	8.2
	NVAE [56]	51.67	5.51
	NCP-VAE [1]	24.08	-
GAN-based methods	AutoGAN [6]	12.4	8.55 ± 0.1
	BigGAN [3]	14.73	9.22
	StyleGAN2 (w/o ADA) [24]	8.32	9.21 ± 0.09
	Progressive GAN [23]	-	8.8
	SNGAN [37]	21.7	8.22
	SNGAN + DDLS [7]	15.42	9.09
Score-based methods	NCSN [52]	25.32	8.87
	NCSNv2 (w/denoising) [53]	10.87	8.40 ± 0.07
	DDPM [21]	3.17	9.46 ± 0.11
	SDE (NCSN++) [54]	2.45	9.73
	SDE (DDPM++) [54]	2.78	9.64
	LSGM (FID) [57]	2.10	-

Table 4: Generative performance on unconditional CIFAR-10

	Method	FID ↓
Ours	DiffuseVAE	4.76
VAE-based methods	NCP-VAE [1]	5.25
	VAEBM [62]	5.31
	NVAE [56]	14.74
Score-based methods	NCSN [52]	25.30
	NCSNv2 [53]	10.23
GAN-based methods	QA-GAN [41]	6.42
	COCO-GAN [34]	4.0

Table 5: Generative performance on CelebA (64 x 64) (t=1000)

samples (Fig. 9 (Top row)). Similarly, on an image denoising task (with noise std=0.1), our model can denoise the corrupted samples (Fig. 9 (Middle row)). Intuitively, these results can be expected since, during training, the proposed DiffuseVAE method learns to refine VAE reconstructions which lack a lot of detail and are inherently blurry. Hence the task of refining these reconstructions might be more challenging than learning to upsample a downsampled version of an image. However, it is worth noting that certain artifacts in the generated reconstructions are evident, leaving scope for improvements.

5.5 State-of-the-art comparisons

Table 4 shows quantitative comparison between DiffuseVAE (Form-1) and other state-of-the-art generative models in terms of the FID [19] and Inception score (IS) [48] on the CIFAR-10 dataset. Apart from score-based models, DiffuseVAE outperforms all state-of-the-art VAE-based methods (which utilize large-dimensional latent hierarchies [56, 62]) and comparably with state-of-the-art GAN-based methods like StyleGAN2 [25] on the CIFAR-10 unconditional image synthesis benchmark. Unsurprisingly, when using half the number of timesteps during the reverse process (i.e. t=500), DiffuseVAE outperforms our unconditional DDPM baseline in terms of FID. We also trained a CIFAR-10 model conditioned on continuous noise as discussed in Section 5.3. We found that for a linear noise schedule between (1e-6, 0.06) and $t = 100$, this model also performed reasonably well compared to other state-of-the-art methods. We observed similar results on the CelebA (64 x 64) benchmark (See Table 5). *To the best of our knowledge, our method is the first to exhibit comparable/superior performance with GANs while utilizing a non-adversarial training setup with a low-dimensional latent space*. Some higher resolution samples (256 x 256) generated from DiffuseVAE are presented in Appendix E.

6 Discussion

In this work, we presented a novel unifying framework for training VAEs and diffusion models. We presented the effectiveness of the proposed approach in generating high-quality samples, requiring fewer reverse process steps during inference when compared with the unconditional DDPM formulation, equipping DDPM with a low dimensional latent code which can be used for controllable synthesis using DDPM, and generalizing to additional tasks like image super-resolution and denoising. However, the DiffuseVAE model is not without its limitations. Due to a generator-refiner framework, the semantics of the final generated samples depends largely on the coarse sample generated by the *generator* model (a simple VAE in our case). Therefore, if the coarse sample is not semantically meaningful, this will

propagate to the final generated sample after refinement. This can be expected from VAE's due to a mismatch between the aggregated posterior $q(z)$ and the prior $p(z)$ during VAE training. Lastly, it would be interesting to experiment with the choice of the VAE network in the first DiffuseVAE stage and observe its impact on the downstream sample quality.

7 Impact Statement

In addition to modelling images, our proposed approach can also be used to model data of other modalities like speech, text, etc. It has the potential to mitigate bias and privacy issues for related ML models that require data collection and annotation. However, such techniques could also be misused to produce fake or misleading information, and researchers should be aware of these risks and explore the proposed approaches responsibly.

Acknowledgements

We would like to thank Ben Poole for his insightful comments and suggestions throughout the course of this project.

References

[1] Jyoti Aneja, Alexander G. Schwing, Jan Kautz, and Arash Vahdat. Ncp-vae: Variational autoencoders with noise contrastive priors. *ArXiv*, abs/2010.02917, 2020.

[2] M. Bauer and A. Mnih. Resampled priors for variational autoencoders. In *Proceedings of the 22nd International Conference on Artificial Intelligence and Statistics (AISTATS)*, volume 89 of *Proceedings of Machine Learning Research*, pages 66–75. PMLR, April 2019. URL `http://proceedings.mlr.press/v89/`.

[3] Andrew Brock, Jeff Donahue, and Karen Simonyan. Large scale gan training for high fidelity natural image synthesis. *arXiv preprint arXiv:1809.11096*, 2018.

[4] Yuri Burda, Roger Grosse, and Ruslan Salakhutdinov. Importance weighted autoencoders, 2016.

[5] Christopher P. Burgess, Irina Higgins, Arka Pal, Loic Matthey, Nick Watters, Guillaume Desjardins, and Alexander Lerchner. Understanding disentangling in β-vae, 2018.

[6] Bing Cao, Han Zhang, Nannan Wang, Xinbo Gao, and Dinggang Shen. Auto-gan: self-supervised collaborative learning for medical image synthesis. In *Proceedings of the AAAI Conference on Artificial Intelligence*, volume 34, pages 10486–10493, 2020.

[7] Tong Che, Ruixiang Zhang, Jascha Sohl-Dickstein, Hugo Larochelle, Liam Paull, Yuan Cao, and Yoshua Bengio. Your gan is secretly an energy-based model and you should use discriminator driven latent sampling, 2021.

[8] Nanxin Chen, Yu Zhang, Heiga Zen, Ron J. Weiss, Mohammad Norouzi, and William Chan. Wavegrad: Estimating gradients for waveform generation, 2020.

[9] Ricky T. Q. Chen, Xuechen Li, Roger Grosse, and David Duvenaud. Isolating sources of disentanglement in variational autoencoders, 2019.

[10] Rewon Child. Very deep vaes generalize autoregressive models and can outperform them on images, 2021.

[11] Jooyoung Choi, Sungwon Kim, Yonghyun Jeong, Youngjune Gwon, and Sungroh Yoon. Ilvr: Conditioning method for denoising diffusion probabilistic models, 2021.

[12] Bin Dai and David Wipf. Diagnosing and enhancing vae models. *arXiv preprint arXiv:1903.05789*, 2019.

[13] Prafulla Dhariwal and Alex Nichol. Diffusion models beat gans on image synthesis, 2021.

[14] Alexey Dosovitskiy and Thomas Brox. Generating images with perceptual similarity metrics based on deep networks, 2016.

[15] Yilun Du and Igor Mordatch. Implicit generation and generalization in energy-based models, 2020.

[16] Partha Ghosh, Mehdi S. M. Sajjadi, Antonio Vergari, Michael J. Black, and Bernhard Schölkopf. From variational to deterministic autoencoders. *ArXiv*, abs/1903.12436, 2020.

[17] Ian J. Goodfellow, Jean Pouget-Abadie, Mehdi Mirza, Bing Xu, David Warde-Farley, Sherjil Ozair, Aaron Courville, and Yoshua Bengio. Generative adversarial networks, 2014.

[18] Will Grathwohl, Ricky T. Q. Chen, Jesse Bettencourt, Ilya Sutskever, and David Duvenaud. Ffjord: Free-form continuous dynamics for scalable reversible generative models, 2018.

[19] Martin Heusel, Hubert Ramsauer, Thomas Unterthiner, Bernhard Nessler, and Sepp Hochreiter. Gans trained by a two time-scale update rule converge to a local nash equilibrium, 2018.

[20] I. Higgins, L. Matthey, A. Pal, Christopher P. Burgess, Xavier Glorot, M. Botvinick, S. Mohamed, and Alexander Lerchner. beta-vae: Learning basic visual concepts with a constrained variational framework. In *ICLR*, 2017.

[21] Jonathan Ho, Ajay Jain, and Pieter Abbeel. Denoising diffusion probabilistic models, 2020.

[22] Jonathan Ho, Chitwan Saharia, William Chan, David J Fleet, Mohammad Norouzi, and Tim Salimans. Cascaded diffusion models for high fidelity image generation. *arXiv preprint arXiv:2106.15282*, 2021.

[23] Tero Karras, Timo Aila, Samuli Laine, and Jaakko Lehtinen. Progressive growing of gans for improved quality, stability, and variation, 2018.

[24] Tero Karras, Samuli Laine, and Timo Aila. A style-based generator architecture for generative adversarial networks, 2019.

[25] Tero Karras, Samuli Laine, Miika Aittala, Janne Hellsten, Jaakko Lehtinen, and Timo Aila. Analyzing and improving the image quality of stylegan, 2020.

[26] Diederik P. Kingma and Prafulla Dhariwal. Glow: Generative flow with invertible 1x1 convolutions. In *NeurIPS*, 2018.

[27] Diederik P Kingma and Max Welling. Auto-encoding variational bayes, 2014.

[28] Diederik P. Kingma, Danilo J. Rezende, Shakir Mohamed, and Max Welling. Semi-supervised learning with deep generative models, 2014.

[29] Diederik P. Kingma, Tim Salimans, Rafal Jozefowicz, Xi Chen, Ilya Sutskever, and Max Welling. Improving variational inference with inverse autoregressive flow, 2017.

[30] Diederik P. Kingma, Tim Salimans, Ben Poole, and Jonathan Ho. Variational diffusion models, 2021.

[31] Alex Krizhevsky. Learning multiple layers of features from tiny images. pages 32–33, 2009. URL `https://www.cs.toronto.edu/~kriz/learning-features-2009-TR.pdf`.

[32] Cheng-Han Lee, Ziwei Liu, Lingyun Wu, and Ping Luo. Maskgan: Towards diverse and interactive facial image manipulation. In *IEEE Conference on Computer Vision and Pattern Recognition (CVPR)*, 2020.

[33] Wonkwang Lee, Donggyun Kim, Seunghoon Hong, and Honglak Lee. High-fidelity synthesis with disentangled representation, 2020.

[34] Chieh Hubert Lin, Chia-Che Chang, Yu-Sheng Chen, Da-Cheng Juan, Wei Wei, and Hwann-Tzong Chen. Coco-gan: Generation by parts via conditional coordinating, 2020.

[35] Eric Luhman and Troy Luhman. Knowledge distillation in iterative generative models for improved sampling speed, 2021.

[36] Vaden Masrani, Tuan Anh Le, and Frank Wood. The thermodynamic variational objective, 2021.

[37] Takeru Miyato, Toshiki Kataoka, Masanori Koyama, and Yuichi Yoshida. Spectral normalization for generative adversarial networks, 2018.

[38] Alex Nichol and Prafulla Dhariwal. Improved denoising diffusion probabilistic models, 2021.

[39] Erik Nijkamp, Mitch Hill, Song-Chun Zhu, and Ying Nian Wu. Learning non-convergent non-persistent short-run mcmc toward energy-based model, 2019.

[40] Anton Obukhov, Maximilian Seitzer, Po-Wei Wu, Semen Zhydenko, Jonathan Kyl, and Elvis Yu-Jing Lin. High-fidelity performance metrics for generative models in pytorch, 2020. URL `https://github.com/toshas/torch-fidelity`. Version: 0.3.0, DOI: 10.5281/zenodo.4957738.

[41] KANCHARLA PARIMALA and Sumohana Channappayya. Quality aware generative adversarial networks. In H. Wallach, H. Larochelle, A. Beygelzimer, F. d Alche-Buc, E. Fox, and R. Garnett, editors, *Advances in Neural Information Processing Systems*, volume 32. Curran Associates, Inc., 2019. URL `https://proceedings.neurips.cc/paper/2019/file/b59a51a3c0bf9c5228fde841714f523a-Paper.pdf`.

[42] Gaurav Parmar, Dacheng Li, Kwonjoon Lee, and Zhuowen Tu. Dual contradistinctive generative autoencoder. In *Proceedings of the IEEE/CVF Conference on Computer Vision and Pattern Recognition*, pages 823–832, 2021.

[43] Adrian Alan Pol, Victor Berger, Gianluca Cerminara, Cecile Germain, and Maurizio Pierini. Anomaly detection with conditional variational autoencoders, 2020.

[44] Ali Razavi, Aaron van den Oord, and Oriol Vinyals. Generating diverse high-fidelity images with vq-vae-2, 2019.

[45] Danilo Jimenez Rezende and Shakir Mohamed. Variational inference with normalizing flows, 2016.

[46] Olaf Ronneberger, Philipp Fischer, and Thomas Brox. U-net: Convolutional networks for biomedical image segmentation, 2015.

[47] Chitwan Saharia, Jonathan Ho, William Chan, Tim Salimans, David J Fleet, and Mohammad Norouzi. Image super-resolution via iterative refinement. *arXiv preprint arXiv:2104.07636*, 2021.

[48] Tim Salimans, Ian J. Goodfellow, Wojciech Zaremba, Vicki Cheung, Alec Radford, and Xi Chen. Improved techniques for training gans. In *NIPS*, 2016.

[49] Samarth Sinha and Adji B. Dieng. Consistency regularization for variational auto-encoders, 2021.

[50] Jascha Sohl-Dickstein, Eric A. Weiss, Niru Maheswaranathan, and Surya Ganguli. Deep unsupervised learning using nonequilibrium thermodynamics, 2015.

[51] Jiaming Song, Chenlin Meng, and Stefano Ermon. Denoising diffusion implicit models, 2021.

[52] Yang Song and Stefano Ermon. Generative modeling by estimating gradients of the data distribution, 2020.

[53] Yang Song and Stefano Ermon. Improved techniques for training score-based generative models, 2020.

[54] Yang Song, Jascha Sohl-Dickstein, Diederik P Kingma, Abhishek Kumar, Stefano Ermon, and Ben Poole. Score-based generative modeling through stochastic differential equations. In *International Conference on Learning Representations*, 2021. URL `https://openreview.net/forum?id=PxTIG12RRHS`.

[55] Casper Kaae Sønderby, Tapani Raiko, Lars Maaløe, Søren Kaae Sønderby, and Ole Winther. Ladder variational autoencoders, 2016.

[56] Arash Vahdat and Jan Kautz. Nvae: A deep hierarchical variational autoencoder, 2021.

[57] Arash Vahdat, Karsten Kreis, and Jan Kautz. Score-based generative modeling in latent space, 2021.

[58] Rianne van den Berg, Leonard Hasenclever, Jakub M. Tomczak, and Max Welling. Sylvester normalizing flows for variational inference, 2019.

[59] Aaron van den Oord, Oriol Vinyals, and Koray Kavukcuoglu. Neural discrete representation learning. In *Proceedings of the 31st International Conference on Neural Information Processing Systems*, NIPS'17, page 6309–6318, Red Hook, NY, USA, 2017. Curran Associates Inc. ISBN 9781510860964.

[60] Aaron van den Oord, Oriol Vinyals, and Koray Kavukcuoglu. Neural discrete representation learning, 2018.

[61] Daniel Watson, Jonathan Ho, Mohammad Norouzi, and William Chan. Learning to efficiently sample from diffusion probabilistic models, 2021.

[62] Zhisheng Xiao, Karsten Kreis, Jan Kautz, and Arash Vahdat. Vaebm: A symbiosis between variational autoencoders and energy-based models, 2021.

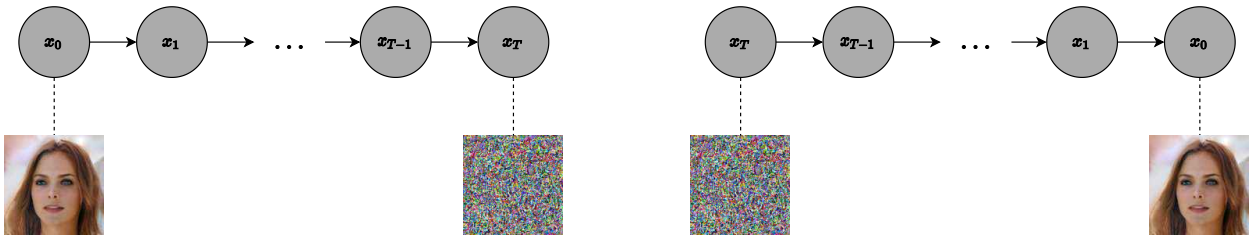

(a) Forward Process

(b) Reverse Process

Figure 10: Illustration of the forward and reverse processes in DDPM

Appendix A: Background on Diffusion models

DDPMs [21, 50] are latent-variable models consisting of a forward noising process ($q(x_{1:T}|x_0)$) (corresponding to an inference model in other generative model families like VAEs [27, 45]. See Fig. 10a) and a reverse denoising process ($p(x_{0:T})$) (corresponding to a generator or decoder in VAEs. See Fig. 10b). The forward process is modeled using a Markov chain which gradually destroys the structure of the data x_0 over a number of timesteps T. Similarly, the reverse process is also modeled as a Markov chain which learns to recover the original data x_0 from the noisy input x_T. The form of the forward process and some notable properties of the forward process conditional distributions are summarized in the following equations (Eqs. (12-18)).

$$q(x_{1:T}|x_0) = \prod_{t=1}^{T} q(x_t|x_{t-1}) \tag{12}$$

$$q(x_t|x_{t-1}) = \mathcal{N}(\sqrt{1-\beta_t}x_{t-1}, \beta_t I) \tag{13}$$

The forward process of DDPMs admits a closed form for x_t for any t, as follows:

$$q(x_t|x_0) = \mathcal{N}(\sqrt{\bar{\alpha}_t}x_0, (1-\bar{\alpha}_t)I) \tag{14}$$

$$\text{where} \quad \alpha_t = (1-\beta_t) \quad \text{and} \quad \bar{\alpha}_t = \prod_t \alpha_t \tag{15}$$

The forward process posteriors are also tractable and are given by

$$q(x_{t-1}|x_t, x_0) = \mathcal{N}(\tilde{\mu}_t(x_t, x_0), \tilde{\beta}_t) \tag{16}$$

$$\text{where} \quad \tilde{\mu}_t(x_t, x_0) = \frac{\sqrt{\bar{\alpha}_{t-1}\beta_t}}{1-\bar{\alpha}_t}x_0 + \frac{\sqrt{\alpha_t}(1-\bar{\alpha}_{t-1})}{1-\bar{\alpha}_t} \tag{17}$$

$$\text{and} \quad \tilde{\beta}_t = \frac{1-\bar{\alpha}_{t-1}}{1-\bar{\alpha}_t}\beta_t \tag{18}$$

The reverse process can also be parameterized using a first-order Markov chain with a learned Gaussian transition distribution as follows

$$p(x_{0:T}) = p(x_T) \prod_{t=1}^{T} p_\theta(x_{t-1}|x_t) \tag{19}$$

$$p_\theta(x_{t-1}|x_t) = \mathcal{N}(\mu_\theta(x_t, t), \Sigma_\theta(x_t, t)) \tag{20}$$

$$p_\theta(x_{t-1}|x_t) = \mathcal{N}(\mu_\theta(x_t, t), \Sigma_\theta(x_t, t)) \tag{21}$$

Given a large enough T and a well-behaved variance schedule of β_t, the distribution $q(x_T|x_0)$ will approximate an isotropic Gaussian. We can generate a new sample from the underlying data distribution $q(x_0)$ by sampling a latent from $p(x_T)$ (chosen to be an isotropic Gaussian distribution) and running the reverse process. As proposed in [21], the

reverse process in DDPM is trained to minimize the following upper bound over the negative log-likelihood (See [50] for detailed proofs):

$$\mathbb{E}_q\left[\mathcal{D}_{KL}(q(x_T|x_0)\|p(x_T)) + \sum_{t>1}\mathcal{D}_{KL}(q(x_{t-1}|x_t,x_0)\|p_\theta(x_{t-1}|x_t)) - \log p_\theta(x_0|x_1)\right] \tag{22}$$

A notable aspect of the above objective is that all the KL divergences involve Gaussians and, consequently, are available in closed form. Notably, [21] parameterize the reverse process conditional $p_\theta(x_{t-1}|x_t)$ using the forward process posterior $q(x_{t-1}|x_t, x_0)$. [21] show that such a parameterization simplifies the second term in Eq. 22 at any given time-step t to the following objective in Eq. 23.

$$\|\epsilon - \epsilon_\theta(\sqrt{\bar{\alpha}_t}x_0 + \sqrt{1-\bar{\alpha}_t}\epsilon, t))\|_2^2 \tag{23}$$

where $x_t = \sqrt{\bar{\alpha}_t}x_0 + \epsilon\sqrt{1-\bar{\alpha}_t}$ and $\epsilon \sim \mathcal{N}(0, I)$. Intuitively, this means that the reverse process in DDPM is trained to predict the noise added to the input x_0 at any time-step t. We use this *simplified* training formulation throughout our work to train all proposed parameterizations of diffusion models as [21] show that this formulation yields superior sample quality than other forms of reverse process parameterizations. For further details on the exact training and inference processes, we encourage the readers to refer to [21].

Appendix B: Detailed Proofs

B.1: Derivation of the DiffuseVAE objective

Given a high-resolution image x_0, an auxiliary conditioning signal y to be modelled using a VAE, a latent representation z associated with y, and a sequence of T representations $x_{1:T}$ learned by a diffusion model, the DiffuseVAE generative process, $p(x_{0:T}, y, z)$ can be factorized as follows:

$$p(x_{0:T}, y, z) = p(z)p_\theta(y|z)p_\phi(x_{0:T}|y, z) \tag{24}$$

where θ and ϕ are the parameters of the VAE decoder and the reverse process of the conditional diffusion model, respectively.The log-likelihood of the training data can then be obtained as:

$$\log p(x_0, y) = \log \int p(x_{0:T}, y, z)dx_{1:T}dz \tag{25}$$

Furthermore, since the joint posterior $p(x_{1:T}, z|y, x_0)$ is intractable to compute, we approximate it using a surrogate posterior $q(x_{1:T}, z|y, x_0)$ which can also be factorized into the following conditional distributions:

$$q(x_{1:T}, z|y, x_0) = q_\psi(z|y, x_0)q(x_{1:T}|y, z, x_0) \tag{26}$$

where ψ are the parameters of the VAE recognition network ($q_\psi(z|y, x_0)$). Since computation of the likelihood in Eq. (25) is intractable, we can approximate it by computing a lower bound (ELBO) with respect to the joint posterior over the unknowns ($x_{1:T}$, z) as:

$$\log p(x_0, y) \geq \mathbb{E}_{q(x_{1:T},z|x_0,y)}\left[\log \frac{p(x_{0:T}, y, z)}{q(x_{1:T}, z|x_0, y)}\right] \tag{27}$$

Plugging the factorial forms of the DiffuseVAE generative process and the joint posterior defined above in eqn. (27), we can simplify the ELBO as follows:

$$\log p(x_0, y) \geq \mathbb{E}_{q(x_{1:T}, z|y, x_0)} \left[\log \frac{p(x_{0:T}, y, z)}{q(x_{1:T}, z|y, x_0)} \right] \tag{28}$$

$$\geq \mathbb{E}_{q(x_{1:T}, z|x_0, y)} \left[\log \frac{p(z) p_\theta(y|z) p_\phi(x_{0:T}|y, z)}{q_\psi(z|y, x_0) q(x_{1:T}|y, z, x_0)} \right] \tag{29}$$

$$\geq \mathbb{E}_{q(x_{1:T}, z|x_0, y)} \left[\log \frac{p(z)}{q_\psi(z|y, x_0)} + \log p_\theta(y|z) + \log \frac{p_\phi(x_{0:T}|y, z)}{q(x_{1:T}|y, z, x_0)} \right] \tag{30}$$

$$\geq \mathbb{E}_{q(z|y, x_0)} \left[\log \frac{p(z)}{q_\psi(z|y, x_0)} + \log p_\theta(y|z) \right] + \mathbb{E}_{q(x_{1:T}, z|x_0, y)} \left[\log \frac{p_\phi(x_{0:T}|y, z)}{q(x_{1:T}|y, z, x_0)} \right] \tag{31}$$

$$\geq \underbrace{\mathbb{E}_{q_\psi(z|y, x_0)} \left[p_\theta(y|z) \right] - \mathcal{D}_{KL}(q_\psi(z|y, x_0) || p(z))}_{\mathcal{L}_{\text{VAE}}} + \mathbb{E}_{z \sim q(z|y, x_0)} \left[\underbrace{\mathbb{E}_{q(x_{1:T}|y, z, x_0)} \left[\frac{p_\phi(x_{0:T}|y, z)}{q(x_{1:T}|y, z, x_0)} \right]}_{\mathcal{L}_{\text{DDPM}}} \right] \tag{32}$$

B.2: Derivation of the DiffuseVAE (Formulation-2) marginals

Given:

$$q(x_1|x_0, \hat{x}_0) = \mathcal{N}(\sqrt{1 - \beta_1} x_0 + \hat{x}_0, \beta_1 I) \tag{33}$$

$$q(x_t|x_{t-1}, \hat{x}_0) = \mathcal{N}(\sqrt{1 - \beta_t} x_{t-1} + (1 - \sqrt{1 - \beta_t}) \hat{x}_0, \beta_t I) \tag{34}$$

From Eqn.(34), we can write,

$$x_t = \sqrt{1 - \beta_t} x_{t-1} + (1 - \sqrt{1 - \beta_t}) \hat{x}_0 + \epsilon \sqrt{\beta_t}, \quad \text{where} \quad \epsilon \sim \mathcal{N}(0, I) \tag{35}$$

Taking expectations both sides,

$$\mathbb{E}(x_t) = \sqrt{1 - \beta_t} \mathbb{E}(x_{t-1}) + (1 - \sqrt{1 - \beta_t}) \hat{x}_0 \tag{36}$$

$$\mathbb{E}(x_t) = \sqrt{1 - \beta_t} \left[\sqrt{1 - \beta_{t-1}} \mathbb{E}(x_{t-2}) + (1 - \sqrt{1 - \beta_{t-1}}) \hat{x}_0 \right] + (1 - \sqrt{1 - \beta_t}) \hat{x}_0$$

$$\mathbb{E}(x_t) = \sqrt{(1 - \beta_t)(1 - \beta_{t-1})} \mathbb{E}(x_{t-2}) + \left(1 - \sqrt{(1 - \beta_t)(1 - \beta_{t-1})} \right) \hat{x}_0$$

$$\vdots \tag{37}$$

$$\mathbb{E}(x_t) = \sqrt{\prod_{t=2}^{t} (1 - \beta_t)} \mathbb{E}(x_1) + \hat{x}_0 \left(1 - \sqrt{\prod_{t=2}^{t} (1 - \beta_t)} \right) \tag{38}$$

Substituting $\mathbb{E}(x_1) = \sqrt{1 - \beta_1} x_0 + \hat{x}_0$ from Eqn.(33) into the above formulation we get,

$$\mathbb{E}(x_t) = \sqrt{\prod_{t=1}^{t} (1 - \beta_t)} x_0 + \hat{x}_0 = \sqrt{\bar{\alpha}_t} x_0 + \hat{x}_0 \tag{39}$$

Similarly it can be shown that $Var(x_t) = (1 - \bar{\alpha}_t) I$. Therefore,

$$q(x_t|x_0, \hat{x}_0) = \mathcal{N}(\sqrt{\bar{\alpha}_t} x_0 + \hat{x}_0, (1 - \bar{\alpha}_t) I) \tag{40}$$

Appendix C: Discussion of DiffuseVAE (Formulation-2)

Algorithm 1 Training (Form. 2)

repeat
  $x_0 \sim q(x_0)$
  $t \sim$ Uniform($\{1 \dots \text{T}\}$)
  $\epsilon \sim \mathcal{N}(0, I)$
  Take gradient descent step on:
    $\nabla_\theta \|\epsilon - \epsilon_\theta(\sqrt{\bar{\alpha}_t}x_0 + \sqrt{1-\bar{\alpha}_t}\epsilon + y, t)\|^2$
until convergence

Algorithm 2 Inference (Form. 2)

$x_T \sim \mathcal{N}(y, I)$
for t = T **to** 1 **do**
  $z = \mathcal{N}(0, I)$, if $t > 1$ else 0
  $\hat{x}_0 = \frac{1}{\sqrt{\bar{\alpha}_t}}(x_t - y - \epsilon_\theta(x_t, y, t)\sqrt{1-\bar{\alpha}_t})$
  $\hat{x}_{t-1} = \gamma_0 \hat{x}_0 + \gamma_1 x_t + \gamma_2 y$
  $x_{t-1} = \hat{x}_{t-1} + z\hat{\sigma}_t$
end for
return $x_0 - y$

The DDPM training objective proposed in [21], has the following form:

$$\mathbb{E}_q \left[\underbrace{\mathcal{D}_{KL}\left(q(x_T|x_0) \| p(x_T)\right)}_{L_T} + \sum_{t>1} \underbrace{\mathcal{D}_{KL}(q(x_{t-1}|x_t, x_0) \| p_\theta(x_{t-1}|x_t))}_{L_{t-1}} - \underbrace{\log p_\theta(x_0|x_1)}_{L_0} \right] \tag{41}$$

Reverse Process parameterization: Following [21], we parameterize the reverse process transition $p_\theta(x_{t-1}|x_t)$ using the functional form of the forward process posterior $q(x_{t-1}|x_t, x_0)$. For the DiffuseVAE formulation proposed in Section 3.4.2 in our paper, the forward process conditional distributions can be specified as:

$$q(x_t|x_{t-1}, \hat{x}_0) = \mathcal{N}\left(\sqrt{1-\beta_t}x_{t-1} + (1 - \sqrt{1-\beta_t})\hat{x}_0, \beta_t I\right) \tag{42}$$

$$q(x_t|x_0, \hat{x}_0) = \mathcal{N}\left(\sqrt{\bar{\alpha}_t}x_0 + \hat{x}_0, (1-\bar{\alpha}_t)I\right) \quad \text{where} \quad t > 1 \tag{43}$$

The posterior distribution $q(x_{t-1}|x_t, x_0, \hat{x}_0)$ will also be a Gaussian distribution with the following form:

$$q(x_{t-1}|x_t, x_0, \hat{x}_0) = \mathcal{N}(\hat{\mu}_t(x_t, x_0, \hat{x}_0), \hat{\beta}_t I) \tag{44}$$

where,

$$\hat{\mu}_t(x_t, x_0, \hat{x}_0) = \underbrace{\frac{\beta_t\sqrt{\bar{\alpha}_{t-1}}}{1-\bar{\alpha}_t}x_0 + \frac{(1-\bar{\alpha}_{t-1})\sqrt{\alpha_t}}{1-\bar{\alpha}_t}x_t}_{\tilde{\mu}_t(x_t, x_0)} + \underbrace{(1 - \frac{(1-\bar{\alpha}_{t-1})\sqrt{\alpha_t}}{1-\bar{\alpha}_t})}_{\kappa}\hat{x}_0 \tag{45}$$

$$\hat{\beta}_t = \frac{(1-\bar{\alpha}_{t-1})}{1-\bar{\alpha}_t}\beta_t \quad \text{and} \quad x_0 = \frac{1}{\sqrt{\bar{\alpha}_t}}(x_t - \hat{x}_0 - \epsilon\sqrt{1-\bar{\alpha}_t}) \quad \text{where} \quad \epsilon \sim \mathcal{N}(0, I) \tag{46}$$

Hence the forward process posterior in this DiffuseVAE formulation is a shifted version of the forward process posterior proposed in [21]. Since the VAE reconstruction $\hat{x}_0$ for an image x_0 is constant during DDPM training, we can parameterize the reverse process posterior as $\hat{\mu}_\theta(x_t, x_0, \hat{x}_0, t) = \tilde{\mu}_\theta(x_t, x_0, t) + \kappa\hat{x}_0$. Additionally, we keep the variance of the reverse process conditional fixed and equal to $\hat{\beta}_t$ as proposed in [21]. Since $L_{t-1} \propto \|\hat{\mu}_t(x_t, x_0, y) - \hat{\mu}_\theta(x_t, x_0, y, t)\|^2$, the DDPM training objective in our formulation remains unchanged from the simplified denoising score matching objective proposed in [21].

Choice of the decoder, L_0: One possible choice for the decoder is to set $p_\theta(x_0|x_1)$ to be a discrete independent decoder derived from the Gaussian $\mathcal{N}(\hat{\mu}_\theta(x_1, \hat{x}_0, 1), \hat{\beta}_1 I)$ [21]. However, at $t = 1$, we have $\hat{\mu}_\theta(x_1, \hat{x}_0, 1) = x_0(x_1, \hat{x}_0, \epsilon_\theta) + \hat{x}_0$. Therefore, to account for the VAE reconstruction bias in the final DDPM output, we set our decoder $p_\theta(x_0|x_1) = \mathcal{N}(\hat{\mu}_\theta(x_1, \hat{x}_0, 1) - \hat{x}_0, \hat{\beta}_1 I)$. Without using this adjustment, we found the final DDPM samples to be a bit blurry in our initial experiments.The final training and inference algorithms are summarized in Algorithms 1 and 2 respectively. In Algorithm 2, the coefficients γ_0, γ_1 and γ_2 denote the coefficients of the forward process posterior in Eqn. 45.

Table 6: Hyperparameters for the training setup in DiffuseVAE. *Cont. Noise* denotes the setting when the Stage-2 DDPM is conditioned on continuous noise as discussed in Section 5.3

		CIFAR-10	**CelebA**	**CelebAMask-HQ**
Stage-I VAE Hyperparameters				
Data	Resolution	32 x 32	64 x 64	128 x 128
	Horizontal Flip	No	No	No
	Data Range	[0, 1]	[0, 1]	[0, 1]
Model	Architecture	See Code	See Code	See Code
	# of parameters	11M	14M	21M
Training	Random Seed	0	0	0
	Mixed Precision	No	No	No
	Effective Batch Size	128	128	128
	# of epochs	500	250	180
	Optimizer	Adam(lr=1e-4)	Adam(lr=1e-4)	Adam(lr=1e-4)
	KL-weight	1.0	1.0	1.0
Stage-II DDPM Hyperparameters				
Data	Resolution	32 x 32	64 x 64	128 x 128
	Horizontal Flip	Yes (for SOTA)	Yes (for SOTA)	No
	Data Range	[-1, 1]	[-1, 1]	[-1, 1]
Model	# of channels	128	128	128
	Scale(s) of attention block	16	16	16
	# of attention heads	1	1	1
	# of residual blocks per scale	2	2	2
	Channel multipliers	(1,2,2,2)	(1,2,2,2,4)	(1,2,2,2,4,4)
	# of parameters	34.4M	84.6M	113M
	Dropout	0.1	0.1	0
	Noise Schedule (default)	Linear(1e-4, 0.02)	Linear(1e-4, 0.02)	Linear(1e-4, 0.02)
	# of timesteps (T)	1000	1000	1000
Training	Random seed	0	0	0
	Mixed Precision	No	No	No
	EMA decay rate	0.9999	0.9999	0.9999
	Effective batch size	128	128	64
	# of epochs	1100	650	250
	Optimizer	Adam(lr=2e-4)	Adam(lr=2e-4)	Adam(lr=2e-5)
	Gradient Clipping Threshold	1.0	1.0	1.0
	# of lr annealing steps	5000	5000	5000
	Diffusion loss type	Noise prediction (L2)	Noise prediction (L2)	Noise prediction (L2)
Evaluation	Variance	fixedlarge	fixedlarge	fixedsmall
	Variance (Cont. noise)	fixedsmall	-	fixedsmall

Appendix D: Training and Hyperparameter details.

All hyperparameters details related to VAE and DDPM training in DiffuseVAE are listed in Table 6

Data preprocessing: For experiments with the CelebAMask-HQ dataset [32], we downsampled the training data to 128 x 128 resolution since we believe this setting provides the correct balance between visual fidelity and training efficiency. We did not use any form of data augmentation during training for the CelebAMask-HQ dataset. However, we used random horizontal flips for experiments involving state-of-the-art comparisons as done in prior work [21]. For all datasets, the training data was scaled between [0.0, 1.0] during the VAE training stage. For Stage-2 DDPM training, the images were scaled between [-1.0, 1.0] for training all DDPM models (including unconditional baselines and DiffuseVAE formulations).

Model architecture: We use the same network architectures as explored in prior work in diffusion models [13, 21, 38]. The VAE architecture used for Stage-1 training consists of residual block architectures inspired from [10] (Refer to our code for exact architectural details). The VAE latent code size was set to 1024 for CelebAMask-HQ and 512 for the

CIFAR-10 and CelebA (64 x 64) datasets. Similar to prior work [21], we use the U-Net [46] decoder implementation from [38] in the reverse process in Stage-II DDPM training. The size of our U-Net model is around 34.4M parameters for CIFAR-10, 84.6M for CelebA (64 x 64) and 113M parameters for the CelebAMask-HQ dataset.

Training: Unless specified otherwise, we use the same hyperparameters during training as proposed in [21]. All DDPM models were trained using the simplified objective proposed in [21]. We used a mix of 4 Nvidia 1080Ti GPUs (44GB memory) and a cloud TPUv2-8 (64GB memory) provided by Colab Pro for training the models.

Evaluation: For FID [19] score computation, we utilized 5k samples for the CelebAMask-HQ dataset and 50k samples for state-of-the-art comparisons on the CIFAR-10 and the CelebA (64 x 64) datasets. We used the torch-fidelity [40] package for FID and IS score computations. In this work, we observed that the FID score also depends on the last de-normalization step when visualizing the image samples. We experimented with two such techniques namely: min-max normalization and standard denormalization (i.e. $0.5 * \text{img} + 0.5$). We used the standard setting for the CIFAR-10, CelebA-64 and the CelebAMask-HQ (with continuous formulations). The samples for all other variants were evaluated using the min-max normalization scheme.

Appendix E: Extended Results

Additional Samples

Some additional DiffuseVAE samples at 256 x 256 resolution and 128 x 128 resolution are visualized in Fig. 11 and Fig. 13 respectively. Additional samples using the continuous noise conditioning formulation of DiffuseVAE's for different inference noise schedules presented in Table 4 in the paper are visualized in Fig. 14. Additional samples for the CelebA and the CIFAR-10 datasets are visualizes in Fig. 12

Controllable synthesis

Some additional results on controllable generation using DiffuseVAE's are visualized in Fig. 15. It is worth noting that we did not fix the DDPM latents as discussed in Section 5.2 when generating these samples. We computed the directions for the vector representing concepts like *Smiling*, *Blonde Hair* and *Black Hair* as discussed in Section 5.2 in the paper.

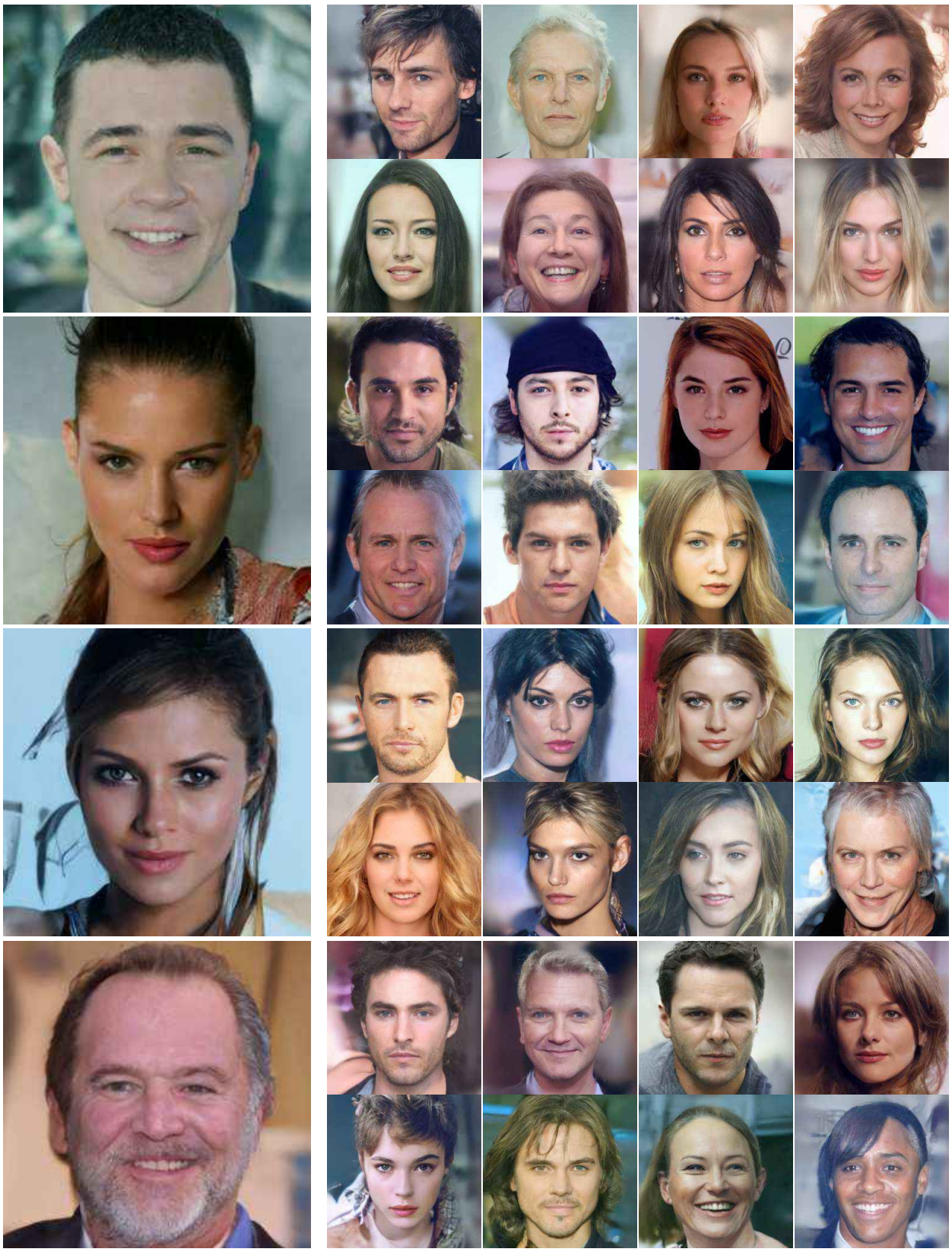

Figure 11: Selected 256 x 256 unconditional samples generated from DiffuseVAE with a latent code size of 1024. DDPM latents are shared between all samples (as explained in Section 5.2) (t=1000, Temp.(λ)=0.8)

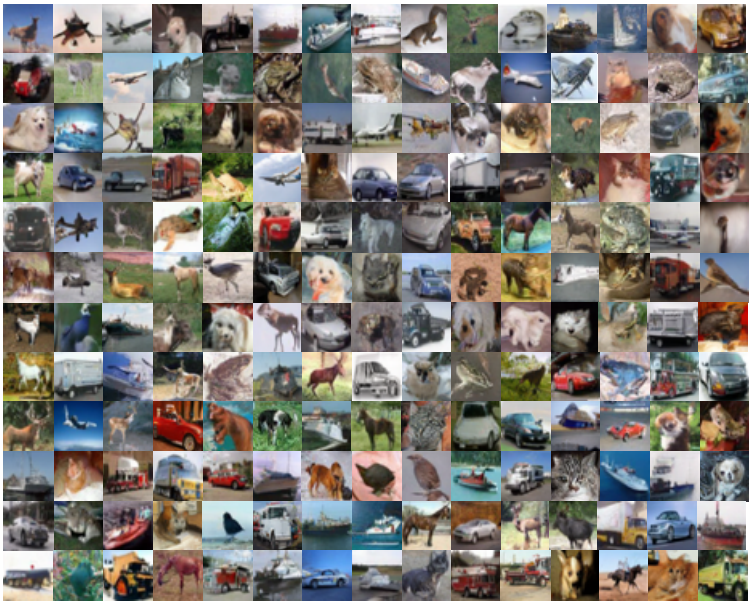

Figure 12: Additional samples from the CelebA and CIFAR-10 datasets generated from DiffuseVAE (t=1000). Both CelebA and CIFAR-10 samples are generated from DiffuseVAE with a latent code size of 512.

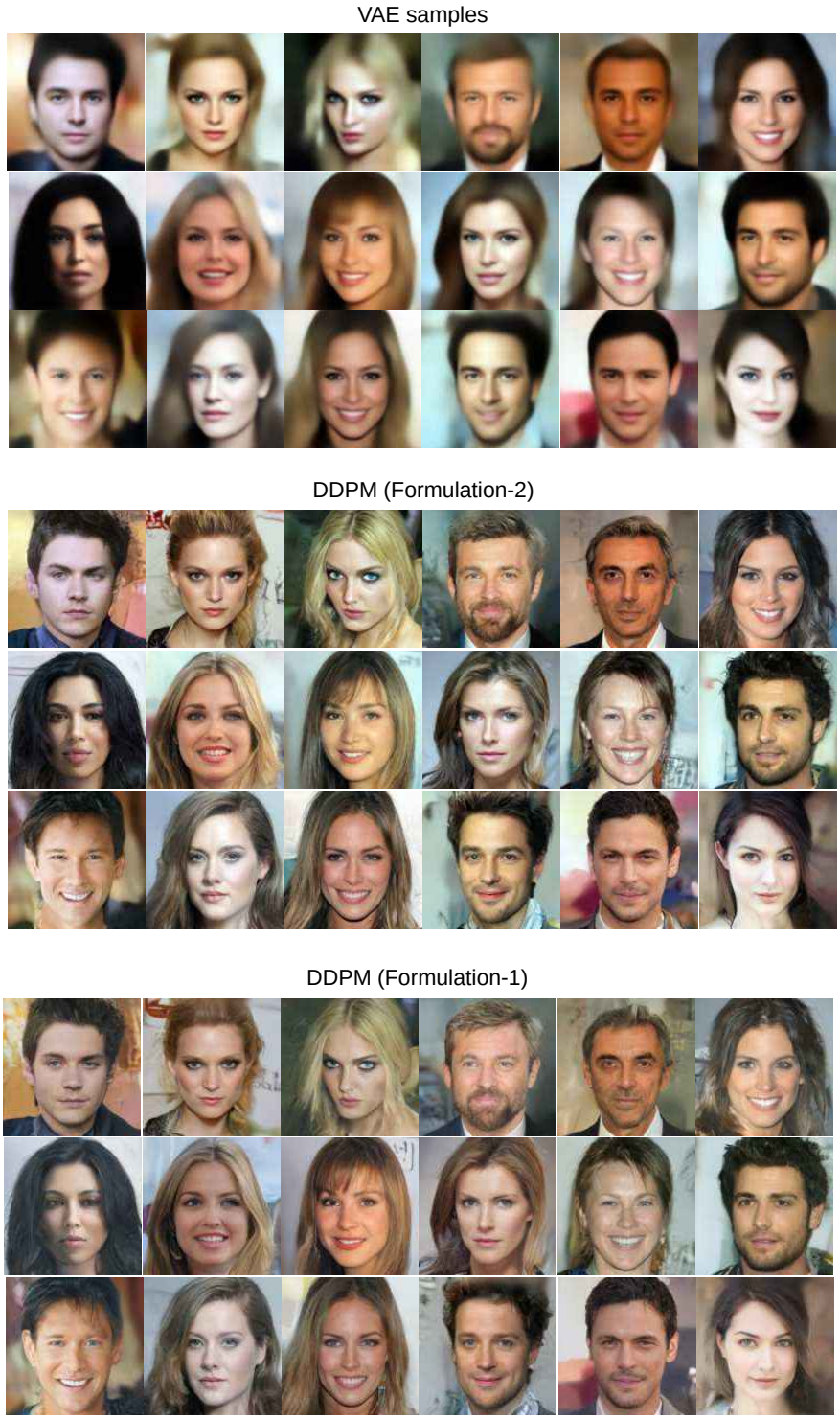

Figure 13: Additional 128 x 128 unconditional samples generated from DiffuseVAE (t=500). Top panel shows the VAE generated unconditional samples and the middle and the bottom panels show the corresponding DDPM refinements.

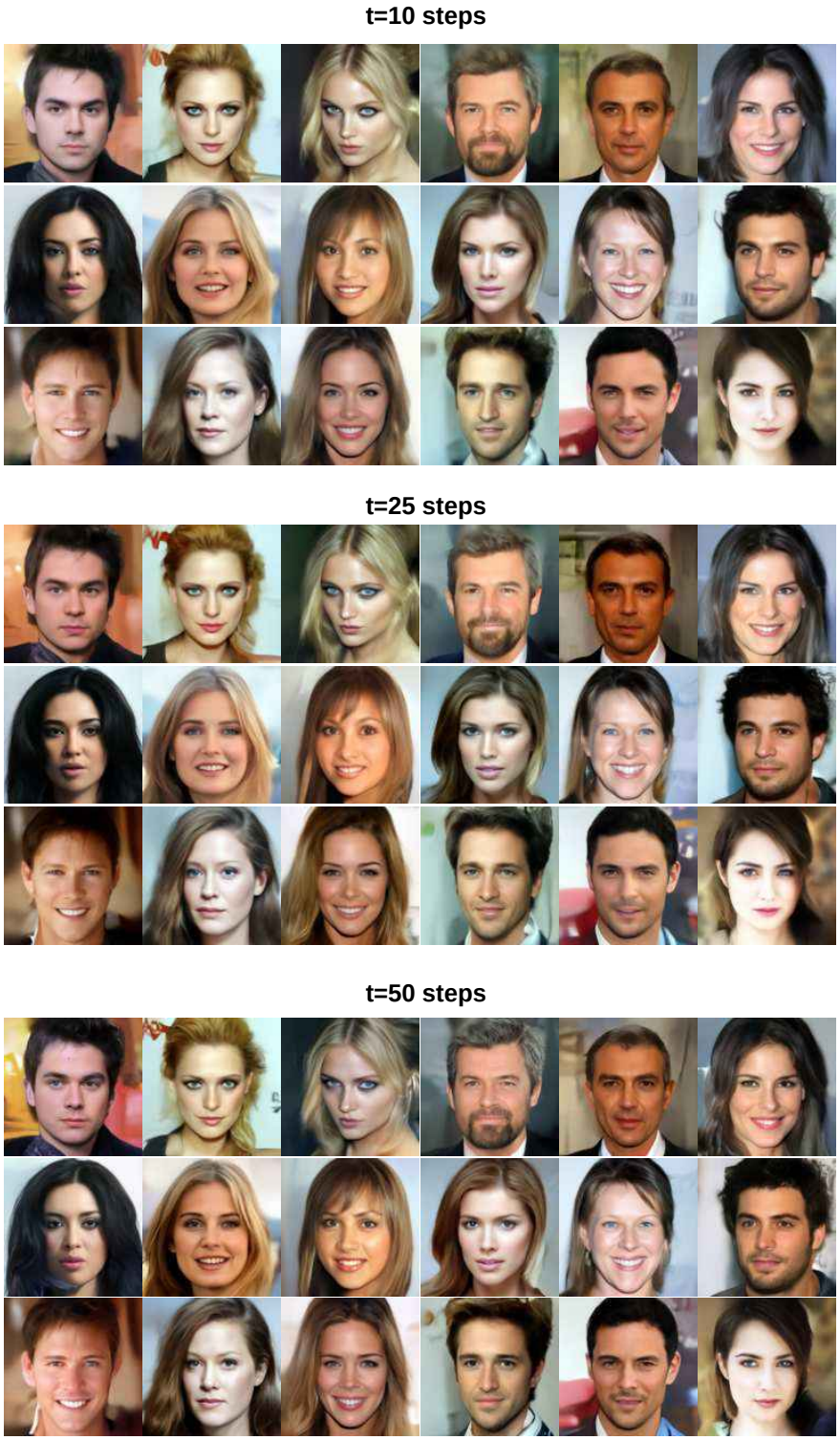

Figure 14: 128 x 128 unconditional samples generated from DiffuseVAE with continuous noise conditioning for inference noise schedules corresponding to Table 4 in the paper. The generated samples are refinements of the VAE samples in Fig. 13

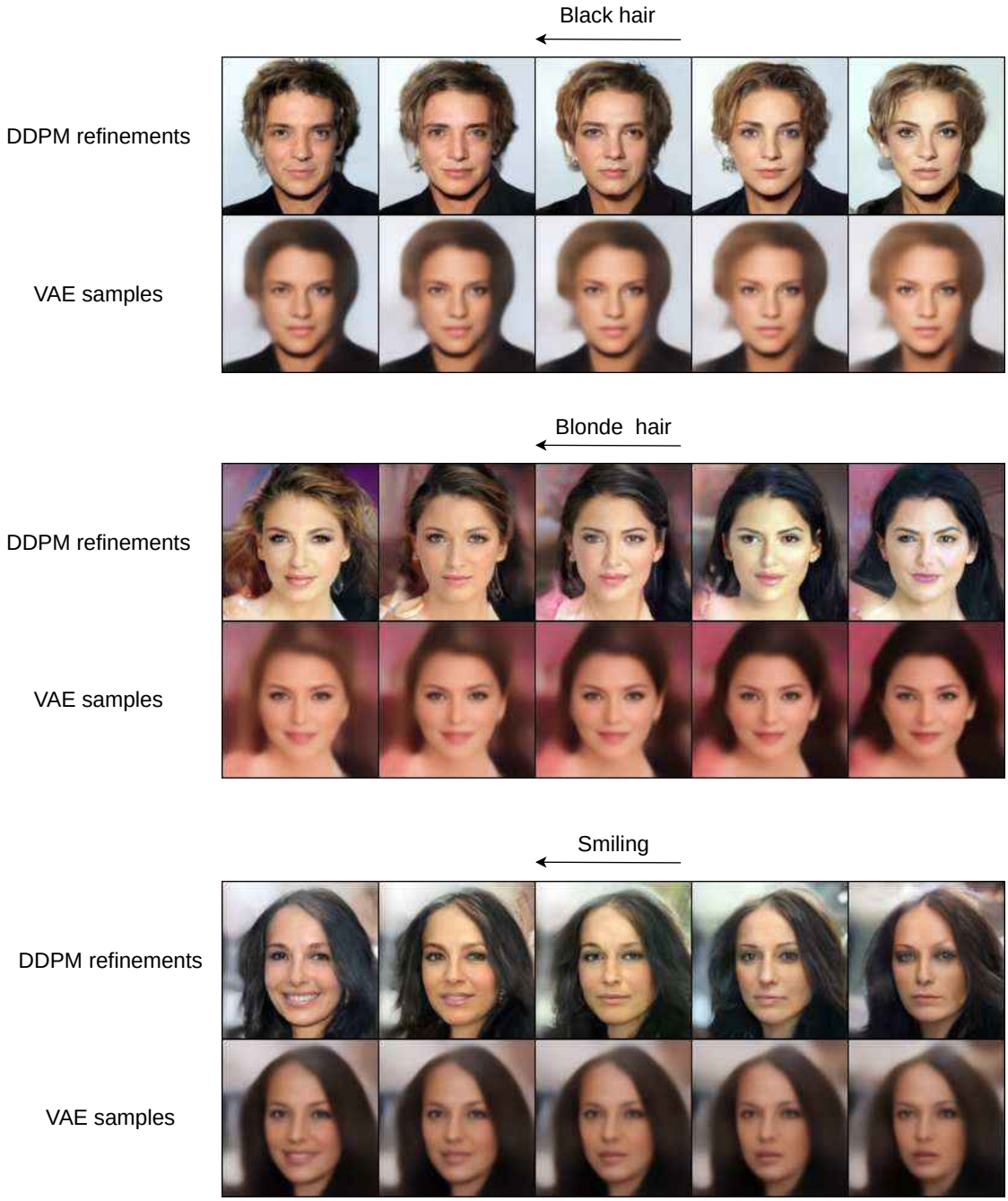

Figure 15: Additional results on controllable synthesis interpolations using DiffuseVAE. DDPM latents are not shared between the interpolations leading to minor differences between the interpolation samples.